Summary: We describe the recent discovery of promising new Ge-based magnetic semiconductors and heterostructures using combinatorial molecular-beam epitaxy for the science and applications of spintronics. We discuss key experimental considerations for implementing combinatorial synthesis and characterization, and highlight important findings in epitaxial films of (100) Ge doped by Co and Mn, specifically the ternary epitaxial phase-diagram, and the novel magnetic and electrical-transport phenomena. We illustrate the natural ''marriage'' between the controlled synthesis and combinatorial approach, and demonstrate the usefulness of the approach for studying complex epitaxial processes.

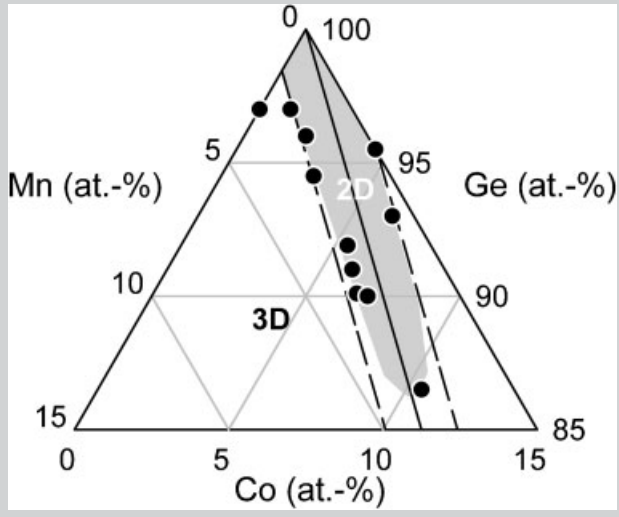

Epitaxial phase-diagram of $Co_xMn_yGe_{1-x-y}$ (100) films.

The Combinatorial Approach: A Useful Tool for Studying Epitaxial Processes in Doped Magnetic Semiconductors

Frank Tsui,[*1] *Yong S. Chu*[2]

[1] Department of Physics and Astronomy, University of North Carolina, Chapel Hill, NC 27599, USA
Fax: (+1) 919 962-0480; E-mail: ftsui@physics.unc.edu
[2] Advanced Photon Source, Argonne National Laboratory, Argonne, IL 60439, USA

Received: October 10, 2003; Revised: November 3, 2003; Accepted: November 4, 2003; DOI: 10.1002/marc.200300188

Keywords: magnetic semiconductors; molecular beam epitaxy; phase diagrams; spintronics; X-ray

1. Introduction

One of the most exciting prospects of materials research is the ability to develop new materials and properties through atomic-scale synthesis.[1] Since its inception in the 1970s, molecular beam epitaxy (MBE) has played a central role in producing artificially structured materials, such as superlattices, quantum wells, and two-dimensional (2D) electron systems, which have led to revolutionary advances, including quantum Hall effects and giant magnetoresistance materials. The essence of MBE is a set of highly controlled techniques operating under ultrahigh vacuum (UHV) conditions, enabling samples to be tailored based on research requirements. The large controllable parameter space, for example growth temperature, deposition rate, composition, thickness, and substrate constraints, also makes MBE a slow process. The conventional one-sample-at-a-time approach for carrying out systematic studies of the epitaxial processes would require a large number of samples to be made and characterized, so the work can be extremely tedious and time consuming. In contrast, the use of a combinatorial approach to vary the same parameters on a single substrate can dramatically enhance the speed to probe the large parameter space and the ability to resolve abrupt transitions.

In the past researchers occasionally employed combinatorial approaches to explore thickness-dependent phenomena, such as interlayer magnetic coupling in magnetic multilayers[2] and magnetic ordering in ultrathin films.[3] Recent advances in instrumentation have extended the approach to compositional dependence and beyond, in order to examine complete phase-diagrams of MBE-grown

ternary systems, thus making it somewhat of an ''art form''.[4–6] In this article we describe how combinatorial MBE was used for the discovery of a promising new class of Ge-based magnetic semiconductors and heterostructures for the science and applications of spin-polarized electronics, ''spintronics''.[7,8] We discuss key experimental considerations for implementing combinatorial synthesis and characterization, and highlight important findings in epitaxial films of (100) Ge doped by Co and Mn, specifically the ternary epitaxial phase-diagram, and the novel magnetic and electrical-transport phenomena. We intend to use this particular material system to illustrate the natural ''marriage'' between the controlled synthesis and combinatorial approach, and to demonstrate the usefulness of the approach for studying complex epitaxial processes.

2. Experimental Techniques

2.1. Combinatorial MBE Synthesis

The synthesis was carried out using an advanced combinatorial MBE system at the University of North Carolina at Chapel Hill (UNC-CH), in which the composition profile across each substrate can be tailored so that properties can be examined as a continuous function of thickness and composition during epitaxial growth.[5,9] As illustrated in Figure 1, this was accomplished by a combination of precision masks and sample manipulation, and real-time flux control using atomic absorption (AA) spectroscopy calibrated in situ by quartz crystal monitors and ex situ by Rutherford backscattering spectroscopy (RBS), X-ray diffraction (XRD)[10,11] and X-ray fluorescence spectroscopy (XFS).[12] A mass spectrometer with appropriate mass range can also be used as a convenient alternative to the AA flux monitors. Each source material requires an AA monitor, which consists of a hollow cathode lamp, a monochromator and a detector, all operating in the UV range of the optical spectrum. The system can accommodate up to eight independently controlled UHV sources, including electron-beam hearths and effusion cells, with a based pressure of about 10^{-11} Torr. The sample holder consists of a six-axis stepper-motor-controlled manipulator designed for in situ diffraction experiments and sample transfer, and a liquid-nitrogen-cooled sample heater with a temperature range between $-100\,^{\circ}C$ and $1300\,^{\circ}C$.

We typically employed a ''multilayer'' method, in which sequential deposition of submonolayer wedges of individual components – Co, Mn, and Ge – was carried out using computer-controlled source shutters and shadow masks, as shown in Figure 1. Both ''binary'' and ''ternary'' samples, with respective linear and planar composition profiles, can be produced in this fashion. The structural evolution of binary samples can be examined using real-time scanning reflection high-energy electron diffraction (RHEED) imaging, and that across ternary samples can be measured in situ using low-energy electron diffraction (LEED) and spectroscopy.

2.2. Structural Analysis Using Microfocused Synchrotron X-rays

Structural analysis using microfocused X-rays was carried out at the X-ray Operation and Research beamlines 2-BM-B, 7-ID-C and 2-ID-E, of the Advanced Photon Source (APS).[10,11] The high brilliance of the APS source delivers a high flux at the focal spot of the beam (1–50 μm), required for the combinatorial studies, while maintaining sufficiently high angular resolution to resolve the epitaxial structures. Instrumentation development of microprobes for hard X-rays is rather advanced at the APS, which currently provides a number of beamlines suited for our research.

We employed Kirkpatrick–Baez (KB) mirrors to produce a microfocused X-ray beam of 5 μm × 12 μm. The size of the beam was kept deliberately much larger than the minimal spot

Frank Tsui is an associate professor of physics and applied and materials science at the University of North Carolina at Chapel Hill. The focus of his research has been atomic scale synthesis and characterization of magnetic thin films and heterostructures using molecular beam epitaxy techniques. He received his BS degree in Engineering Physics from the University of California at Berkeley in 1984, and his MS (1987) and Ph.D. (1992) degrees in physics from the University of Illinois at Urbana-Champaign, where he was an IBM Predoctoral Fellow. He was a Margaret and Herman Sokol Postdoctoral Fellow in the Sciences at the University of Michigan at Ann Arbor, before he joined the faculty of the University of North Carolina in 1995 as an assistant professor of physics. He was a recipient of the US National Science Foundation CAREER award in 1997.

Yong Chu is a beamline scientist at the Advanced Photon Source (APS) in Argonne National Laboratory. His research interests include the investigation of interfacial structures at surfaces using x-ray scattering and the development of synchrotron instrumentation. As a member of the X-ray Microscopy Group at APS, he is currently developing x-ray diffraction microscopy techniques. In particular, he has developed high-throughput characterization techniques for combinatorial materials using scanning x-ray microprobe. He received his BS degree in physics from the California Institute of Technology in 1989 and his Ph.D. degree in physics from the University of Illinois at Urbana-Champaign in 1997. He was a postdoctoral research fellow at Argonne National Laboratory from 1997 to 2000.

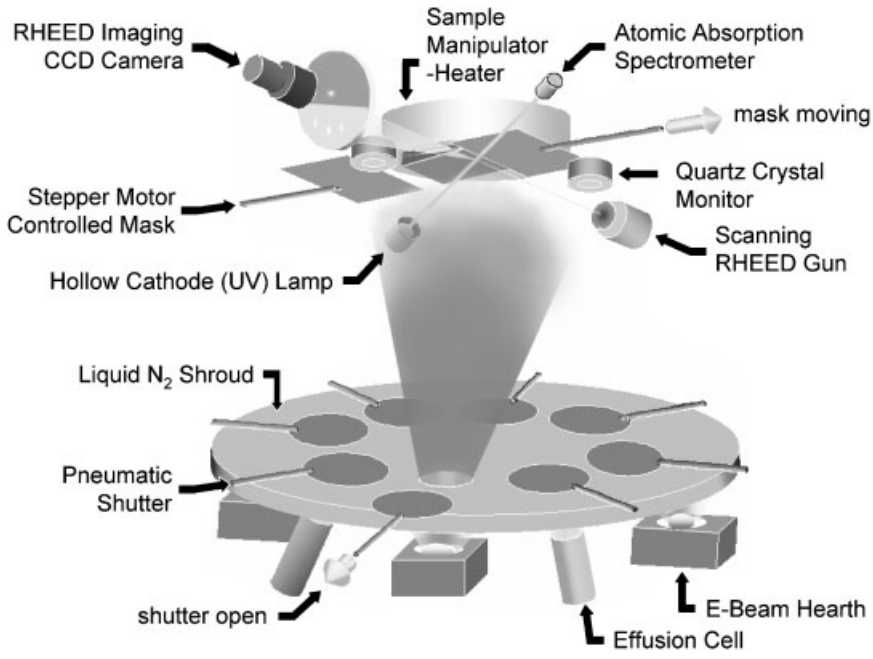

Figure 1. Schematic diagram of the combinatorial MBE system at UNC-CH. The diagram depicts the process of depositing a linear composition profile (the wedge-shaped film mounted on the bottom of the sample manipulator) using a combination of a precision mask (underneath the sample) and a pneumatic shutter (on top of the liquid N_2 shroud above the sources). The speed of the computer-controlled stepper motor and the associated shutter ''exposure'' time are determined by the signal from the atomic absorption (AA) flux monitor. The RHEED beam can be scanned across the sample during growth and annealing with the diffraction patterns on the phosphors screen captured by a CCD camera. The growth and characterization processes are synchronized and controlled by computers.

size for this particular instrument (ca. 1 μm) in order to obtain a high angular resolution for the diffraction measurements and a long focal length ($\geq$ 50 cm) to provide ample space for the wide range of sample rotation necessary for reciprocal space mapping. In order to avoid possible sample oxidation caused by the intense radiation, an inert N_2 environment was maintained around the sample during experiments.

We simultaneously carried out XRD and XFS experiments using one sample coordinate system for examining both the lattice structure and composition.[12] A compact Peltier-cooled Si-drift diode energy-dispersive detector was used for detecting the fluorescence signal instead of a commonly used liquid N_2-cooled Ge detector, in order to provide the additional experimental flexibility needed for the two types of measurements. Simultaneous measurement of lattice structure and composition under the same experimental conditions is important not only for achieving high-throughput characterization but also for eliminating systematic experimental errors associated with transporting samples between two separate experimental stations.

3. Continuous Phase-Diagram of Ge-Based Magnetic Semiconductors

The key bottleneck for the science and application of spintronics[13,14] is the lack of suitable materials. The most desirable materials are those with high-temperature ferromagnetism, and yet are semiconducting and compatible with Si-based processing. The intrinsic difficulty, however, lies in the heavy doping required for achieving a high Curie temperature, T_C, which, in turn, can lead to many detrimental consequences, such as high conductivity, phase separation, and disorder. Recently we have made significant advances in overcoming these materials issues through non-equilibrium MBE synthesis,[7,11] and have demonstrated that by complementary doping using two or more transition metal elements, a range of desirable ''compensation'' effects can be achieved at relatively high doping concentrations, including stable 2D epitaxial growth, suppression of phase separation, shallow impurity levels, and low carrier concentrations. A novel magnetic diode has also been made using these materials,[8] illustrating their viability. In the following sections we highlight some of the key findings from the work. We demonstrate that by using only a limited number of binary combinatorial samples, ternary epitaxial phase-diagrams with sharp transitions can be studied systematically. In contrast, in order to achieve a comparable compositional resolution (ca. 0.1 at.-%) using conventional techniques, about 100 samples would have to be synthesized for each binary sample under growth conditions that are intrinsically less uniform. Therefore, our approach

increases throughput by a factor of a hundred over the conventional approach, and, more importantly, it significantly enhances our control of the synthetic conditions and thus our ability to resolve sharp features in the phase diagram.

3.1. Epitaxial Phase Diagram

Complementary doping using several impurities has long been used for fine-tuning the electronic structures of semiconductors.[15] Its effects on structure have not been studied systematically, particularly for doping level beyond several at.-%. Recently we carried out a systematic study of complementary doping using Co- and Mn-doped Ge (100) as a model system.[11] A series of binary samples were grown by combinatorial MBE at a growth temperature of 250 °C and rate of about 0.1 Å · s^{-1}, and studied by real-time RHEED, XRD, XFS, scanning tunneling microscopy (STM), and cross-sectional high-resolution transmission electron microscopy (HRTEM) experiments. The resulting epitaxial phase diagram in the doping range between 0 and 15 at.-% is shown in Figure 2.

As shown in Figure 2(a), the growth of lightly doped Ge (100) is two dimensional and pseudomorphic, which persists up to a doping concentration indicated by the circles. Above this concentration a transition to rough three-dimensional growth, lattice relaxation and phase separation occurs. The observed transition is sensitive to the relative doping concentration, such that coherent two-dimensional epitaxial growth occurs within a narrow window of composition [the gray area in Figure 2(a)] around a relative doping concentration between Co and Mn of about 3 (the solid line) up to a combined maximum doping of close to 15 at.-%. It is within this regime where promising Ge magnetic semiconductors were discovered with T_C's approaching room temperature,[7] as discussed in the next section. The 2D films are stable under post-growth annealing at temperatures up to 600 °C, above which phase separation occurs. Outside the 2D regime the films are rough, defective, and inhomogeneous.

The phase diagram, shown in Figure 2(a), suggests that lattice mismatch plays an important role. Since the tetrahedral radius of Co is smaller than that of Ge, while that of Mn is larger, complementary doping of the two could compensate the strain effects from each other within a range up to a critical value, as indicated by the dashed lines in Figure 2(a). This idea was further examined using samples with doping profiles like the one indicated by the dashed line connecting ABCD in Figure 2(a). Figure 2(b) and 2(c) show the corresponding RHEED intensity and lattice strain as a function of doping concentrations, respectively. The former corresponds to surface morphology and the latter corresponds to the strain values with respect to that of Ge determined by XRD analysis and corrected for the tetragonal lattice distortion due to pseudomorphic growth.[16]

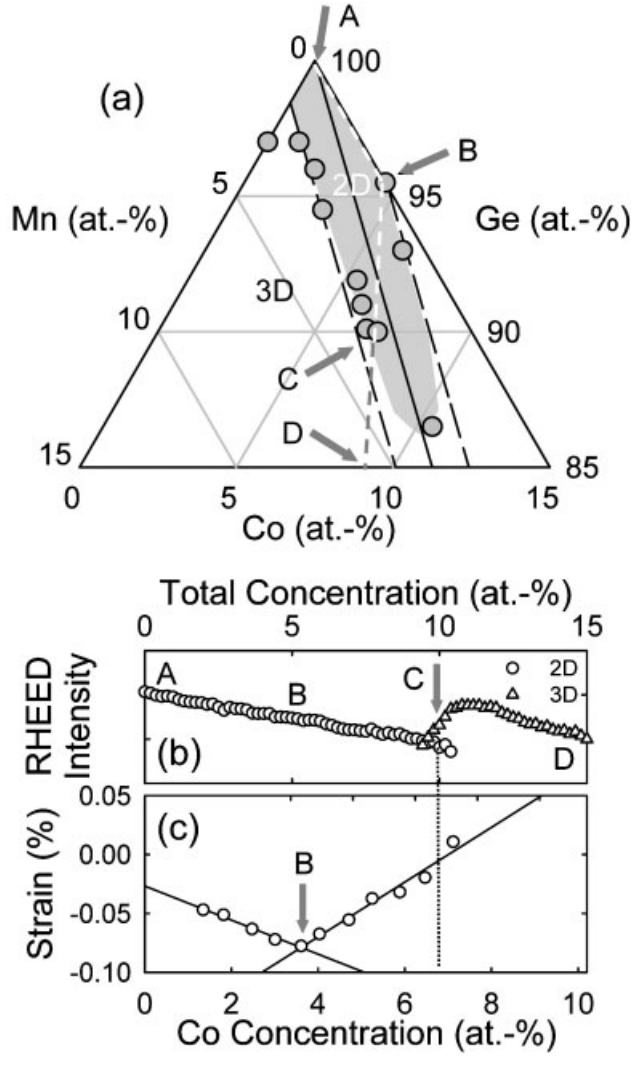

Figure 2. Epitaxial phase-diagram of $Co_xMn_yGe_{1-x-y}$ (100) films. (a) Roughening/disorder transition as a function of doping concentration is indicated by circles with the gray area indicating the region of smooth 2D epitaxial growth. The solid line indicates relative doping concentration between Co and Mn, $x/y \approx 3$, where the intrinsic strains due to Co and Mn substitutional doping are fully compensated. The long dashed lines, on the other hand, mark the boundary where the strain reaches ±0.07%, as discussed in the text [Equation (1)]. The short dashed line connecting ABCD (as indicated by the arrows) indicates the composition profile of the structural results shown in (b) and (c). (b) Surface morphology as a function of total doping concentration, as determined by integrated RHEED intensity. Circles are for the specular intensity of a 2D surface, and triangles are the corresponding 0th order feature of a 3D surface. The arrow indicates the roughening transition at C. (c) Lattice mismatch between the doped Ge film and Ge substrate as a function of Co doping concentration. The strain values were determined by analyzing the XRD results using a simple kinematic model and corrected for the tetragonal distortion due to the in-plane stress.[11,16] The arrow indicates the onset of lattice compensation effect as a result of the onset of Mn doping at B. The dotted line indicates the transition to rough and disordered growth.

The result shown in Figure 2(c) establishes that within the 2D regime the lattice spacing obeys Vegard's law, such that the expansion due to Mn substitutional doping is compensated by the compression due to Co doping, with the net strain, ε, in alloys of $Co_xMn_yGe_{1-x-y}$ given by Equation (1).

$$\varepsilon = -0.015x + 0.045y \quad (1)$$

Here the two terms on the right-hand side correspond to the effects from Co and Mn doping, respectively. The tetrahedral covalent radii obtained from these values are 1.20 Å for Co and 1.27 Å for Mn using the Ge value of 1.22 Å, in excellent agreement with those from recent studies.[17]

Equation (1) further establishes that, at a relative doping concentration x/y of about 3 [solid line in Figure 2(a)], the strain is fully compensated so the doped film is most stable. Here the transition may depend solely on the intrinsic energetics of phase separation. As x/y deviates from this value, $|\varepsilon|$ increases, and when it reaches a critical value Δ (dashed lines in Figure 1e with $\Delta \approx 0.07\%$) and beyond, growth becomes unstable, and surface roughening and disorder occur.

Further analysis of the transition as a function of film thickness[11] reveals that generation of interfacial defects plays a dominant role in controlling the phase separation and strain-relaxation processes. The presence of a solubility gap that promotes the tendency for phase separation, even in the absence of strain, would give rise to a positive solid mixture energy.[18] The energy cost for the system to remain in solid solution is balanced by the energy associated with the generation of interfacial defects. The two energies are comparable at a thickness where generation of interfacial defects becomes viable and thus homogeneous epitaxial growth becomes unstable. The presence of strain would further reduce the stability of epitaxial growth, since the strain energy depends on ε^2.[19–22] In short, our combinatorial study demonstrates that defect-free pseudomorphic growth, with lattice strain fully compensated, resists phase separation, while defective growth and presence of lattice mismatch would trigger the earlier onset of disorder and inhomogeneity. In the next section we describe the novel magnetic and electrical-transport phenomena in a combinatorial sample with the strain nearly compensated.

3.2. Magnetic and Transport Phenomena

$Co_xMn_yGe_{1-x-y}$ alloys order ferromagnetically, with T_C and the saturation magnetization, M_s, increasing with doping concentration, as shown in Figure 3.[7] The M_s values correspond to an average moment per dopant ion of about 0.3 μ_B, which is about 10 times smaller than the known values for Co and Mn but comparable to those observed in some Mn-doped systems,[23] indicating that only a fraction of dopants participate in the ordering. Like its structural counterparts, the magnetism is also sensitive to doping concentration and synthesis conditions. The highest T_C achieved thus far for semiconductors is about 270 K at $x/y \approx 3$ and $x + y \approx 15$ at.-%.

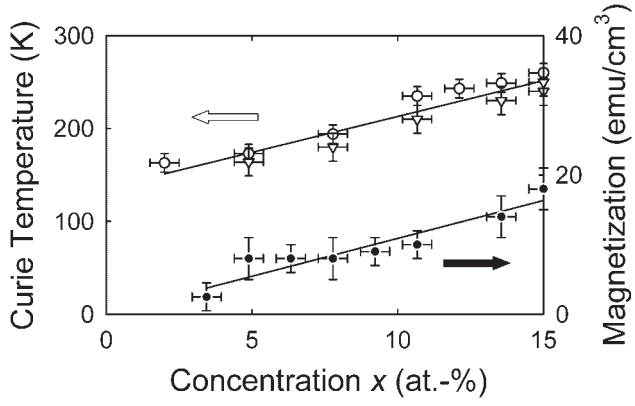

Figure 3. Magnetism of $Co_{0.7x}Mn_{0.3x}Ge_{1-x}$ epitaxial films as a function of doping concentration x. Values of T_C (open symbols) and saturation magnetization M_s (closed circles) versus x were determined by SQUID magnetometry (triangles) and by magnetotransport parameters (circles). The lines are to guide the eyes. The large uncertainties are due to small sample size.

The observed electrical transport phenomenon within the structural 2D regime exhibits the characteristics of a highly doped p-type Ge with a shallow acceptor level of about 30 meV,[7] which is surprisingly low when compared to the known values for Co and Mn (> 160 meV above the valence band).[24,25] Co also has a donor level in Ge about 90 meV above the valence band that can give rise to compensation effects.[25] In fact, carrier concentration estimated from the ordinary Hall coefficient at room temperature varies from 5×10^{17} cm^{-3} to 5×10^{19} cm^{-3}, about 1000-times smaller than the respective doping concentrations, indicating that the alloys are indeed highly compensated. Random distribution of the Co donor impurities also represents a fluctuating potential that can cause broadening of the impurity band[26] in addition to the broadening and perhaps splitting caused by the high doping level and the presence of exchange interactions.

As shown in Figure 4, the temperature-dependent resistivity as a function of doping concentration for a series of $Co_xMn_yGe_{1-x-y}$ alloys with $x/y \approx 2$ exhibits a continuous transition from semiconducting behavior at low concentration to that of a metal with finite resistivity at zero temperature around a doping concentration of about 10 at.-%. The former exhibits a Mott exp $(T^{-1/4})$ temperature dependence, which is associated with a sign change in the ordinary Hall coefficient, indicating the presence of a significant impurity band conduction and that the variable range hopping is the dominant mechanism for transport in the impurity band. The observed semiconductor-metal transition is surprisingly similar to disordered metal-Ge alloys.[28] The key difference here is that, in

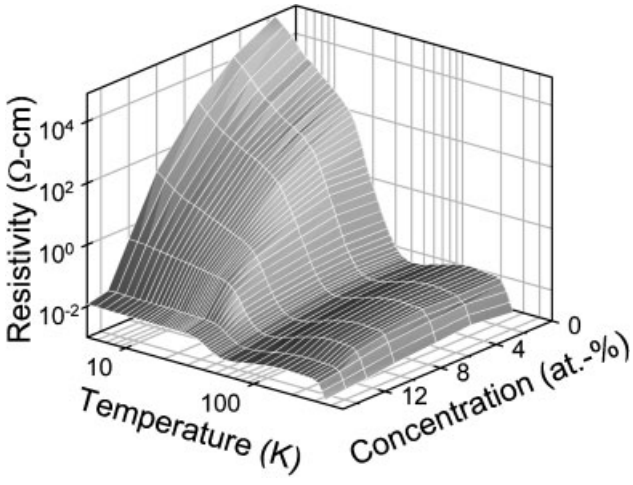

Figure 4. Resistivity of $Co_{0.7x}Mn_{0.3x}Ge_{1-x}$ as a function of temperature and total doping concentration. At low doping concentrations, the temperature-dependent behavior corresponds to that of a highly doped semiconductor with a shallow impurity level,[24] and the low-temperature behavior indicates that variable range hopping in the impurity band dominates the conduction process. A continuous transition to metallic behavior with finite resistivity at zero temperature occurs near the roughening/disorder transition (ca. 10 at.-%).

addition to low-temperature transport phenomena, the doping concentration also controls the magnetism.

The Hall mobility was also estimated. At room temperature, it ranges from 10^3 to 10^2 cm^2/V-s with respect to doping level from 1 to 15 at.-%, and as the temperature decreases it rises to a peak of well above 10^4 cm^2/V-s, before falling by a factor of more than 100 at lower temperatures. The observed high values at low doping levels are comparable to those observed in high purity Ge, indicating the presence of a long carrier mean-free-path that is consistent with the high structural quality of the material. In contrast, the low temperature counterparts confirm the presence of impurity band conduction.

Finally, at temperatures above the hopping regime, the magnetization-dependent Hall effect[27] exhibits a linear correlation with resistivity. This correlation indicates that the carrier relaxation is very weak in this regime, leading to plane-wave states and thus giving rise to the classical skew scattering. This observation, when combined with features like the shallow impurity level, large magnetoresistance effect, high T_C, and compatibility with Si, makes the material quite desirable for exploring spintronics. The viability of the system has been further demonstrated by the recent observation of a large, magnetization-dependent rectification effect in heterojunction diodes made from these materials.

3.3. Magnetic Heterojunction

One type of such heterojunction has been made using Ge magnetic semiconductors (M-Ge) grown epitaxially on lightly doped *n*-type Ge (100) substrates (*n*-Ge), as shown in Figure 5, demonstrating a magnetization-dependent rectification effect.[8] The effect deteriorates for doping levels above 10 at.-%, and it is absent in samples grown on *p*-type and undoped Ge substrates. At low temperatures the observed magnetization-dependent rectification is very large. For instance, the current rectification decreases by a factor of ten in a low field of 200 Oe from its zero-field value. This has been attributed to effects of electron spin-polarization in the impurity band. The large effect and the low field for producing it, when combined with the compatibility with Si, make this type of diode scientifically and technologically relevant.

4. Conclusion

We have discussed recent advances in combinatorial MBE synthesis and characterization leading to the discovery of a

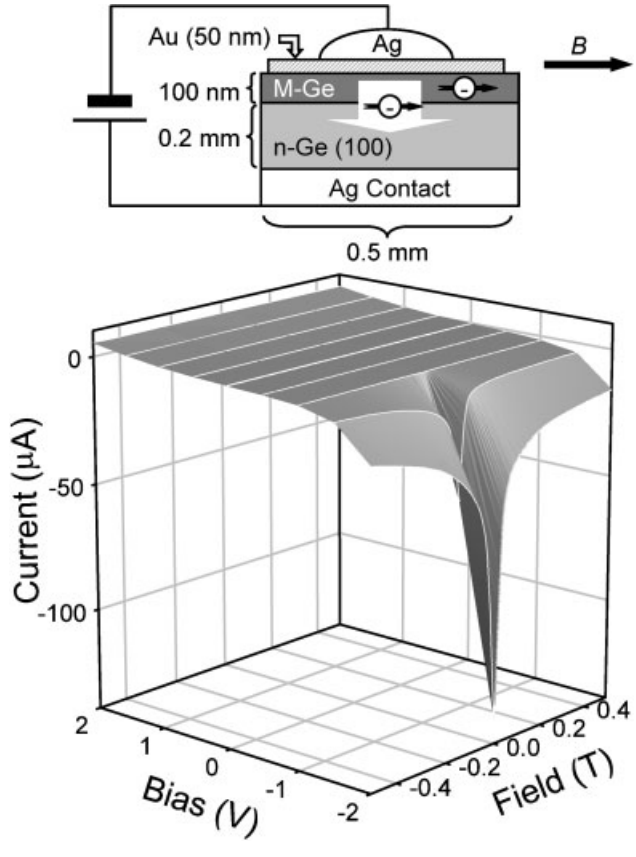

Figure 5. Magnetization-dependent rectification effect in a Ge-based magnetic semiconductor heterojunction. Top: schematic diagram of the heterojunction. Bottom: Characteristic current-voltage curves of the rectifier as a function of magnetic field at 5 K for a M-Ge layer of $Co_{0.03}Mn_{0.01}Ge_{0.96}$ grown epitaxially on lightly doped *n*-type Ge substrate. Below T_C and under back-bias and zero-field, electrons are injected into the *n*-Ge substrate, the ''on'' state, and the ''off'' state corresponds to either forward bias or high field.

new class of promising magnetic semiconductors. The use of a combinatorial approach was instrumental for carrying out the systematic study of the epitaxial phase-diagram, resolving sharp order-disorder and the corresponding metal-semiconductor transitions, while using only a limited number of binary samples. The utility of the approach over the conventional one-sample-at-a-time approach in dealing with these complexes and interrelated epitaxial phenomena is quite evident. The observed compensation effects can also, in turn, help with the design of future experiments involving highly doped systems. However, many results reported here, such as electrical transport and magnetization measurements, still rely on one-sample-at-a-time measurements, so the bottleneck for combinatorial research remains to be the available scanning and imaging characterization techniques. The challenge for the field, therefore, is to develop more and faster quantitative techniques.

Acknowledgements: We thank *Liang He* at UNC-CH, *Andrei Tkachuk*, *Stefan Vogt*, and *Don Walko* at APS, *Toyohiro Chikyow* at the National Institute for Materials Science, Japan, for their collaboration in the research. The work was supported in part by the *US National Science Foundation* DMR-0108605. Use of the Advanced Photon Source was supported by the *U.S. Department of Energy*, Office of Science Basic Energy Sciences, under Contract No. W-31-109-ENG-38.

[1] Committee on Condensed-Matter and Materials Physics, National Research Council, "*Condensed-Matter and Materials Physics: Basic Research for Tomorrow's Technology*", National Academy Press, Washington, D.C. 1999.
[2] J. Unguris, R. J. Celotta, D. T. Pierce, *Phys. Rev. Lett.* **1991**, *67*, 140.
[3] Z. Q. Qiu, J. Pearson, S. D. Bader, *Phys. Rev. Lett.* **1991**, *67*, 1646.
[4] I. Takeuchi, R. B. van Dover, H. Koinuma, *MRS Bulletin* **2002**, *27*, 311.
[5] Y. K. Yoo, F. Tsui, *MRS Bulletin* **2002**, *27*, 316.
[6] Y. Matsumoto, H. Koinuma, T. Hasegawa, I. Takeuchi, F. Tsui, Y. K. Yoo, *MRS Bulletin* **2003**, *28*, 734.
[7] F. Tsui, L. He, L. Ma, A. Tkuchuk, Y. S. Chu, K. Nakajima, T. Chikyow, *Phys. Rev. Lett.* **2003**, *91*, 177203.
[8] F. Tsui, L. Ma, L. He, *Appl. Phys. Lett.* **2003**, *83*, 954.
[9] [9a] F. Tsui, P. A. Ryan, *Appl. Surf. Sci.* **2002**, *189*, 334; [9b] F. Tsui, L. He, L. Ma, MRS Symposium Proceedings, Vol. 700, "*Combinatorial and Artificial Intelligence Methods of Materials Science*", I. Takeuchi, J. M. Newsam, L. T. Wille, H. Koinuma, E. J. Amis, Eds., MRS, Pittsburgh, PA 2001, p. S2.2.1-6.
[10] Y. Chu, A. Tkachuk, S. Vogt, P. Ilinski, D. Walko, D. Mancini, E. Dufresne, L. He, F. Tsui, *Appl. Surf. Sci.* **2004**, in press.
[11] F. Tsui, L. He, A. Tkuchuk, S. Vogt, Y. S. Chu, *Phys. Rev. B*, in press.
[12] S. Vogt, Y. S. Chu, A. Tkachuk, P. Iliniski, D. A. Walko, F. Tsui, *Appl. Surf. Sci.* **2004**, in press.
[13] G. A. Prinz, *Phys. Today* **1995**, *48*, 58.
[14] S. Das Sarma, *American Scientist* **2001**, *89*, 516.
[15] E. H. Putley, "*The Hall Effect and Semiconductor Physics*", Butterworth, London 1960, Chapter 5.
[16] The correction factor for the tetragonal distortion is $(1 + v)/(1 - v)$ for the (100) system with a Poisson ratio, v, of 0.27 for Ge.
[17] R. K. Iwanowski, K. Lawniczak-Jablonska, Z. Golacki, A. Traverse, *Chem. Phys. Lett.* **1998**, *283*, 313.
[18] C. Kittel, H. Kroemer, "*Thermal Physics*", Freeman, San Francisco 1980, Chapter 11.
[19] J. H. Van der Merwe, C. A. B. Ball, in: "*Epitaxial Growth*", J. W. Matthews, Ed., Academic, New York 1975, part B, Chapter 6.
[20] [20a] J. W. Matthews, A. E. Blakeslee, *J. Cryst. Growth* **1974**, *27*, 118; [20b] J. W. Matthews, A. E. Blakeslee, *J. Cryst. Growth* **1976**, *29*, 273.
[21] R. People, J. C. Bean, *Appl. Phys. Lett.* **1985**, *47*, 322.
[22] R. C. Cammarata, *Prog. Surf. Sci.* **1994**, *46*, 1.
[23] H. Ohldag, V. Solinus, F. U. Hillebrecht, J. B. Goedkoop, M. Finazzi, F. Matsukura, H. Ohno, *Appl. Phys. Lett.* **2000**, *76*, 2928.
[24] H. Fritzsche, *Phys. Rev.* **1955**, *99*, 406.
[25] H. H. Woodbury, W. W. Tyler, *Phys. Rev.* **1955**, *100*, 659.
[26] O. Madelung, "*Introduction to Solid State Theory*", Springer, Berlin 1981, Chapter 10.
[27] C. M. Hurd, "*The Hall Effect in Metals and Alloys*", Plenum, New York 1972.
[28] B. W. Dodson, W. L. McMillan, J. M. Mochel, R. C. Dynes, *Phys. Rev. Lett.* **1981**, *46*, 46.

